Available online at www.sciencedirect.com
ScienceDirect
Trans. Nonferrous Met. Soc. China 31(2021) 2703−2715
Transactions of Nonferrous Metals Society of China
www.tnmsc.cn

New insights into microstructural changes during transient liquid phase bonding of GTD-111 superalloy

Javad ASADI[1], Seyed Abdolkarim SAJJADI[1], Hamid OMIDVAR[2]

1. Materials and Metallurgical Engineering Department, Faculty of Engineering, Ferdowsi University of Mashhad, Mashhad, Iran;
2. Department of Materials and Metallurgical Engineering, Amirkabir University of Technology (Tehran Polytechnic), Tehran, Iran

Received 31 October 2020; accepted 18 June 2021

Abstract: The effects of joining temperature (T_J) and time (t_J) on microstructure of the transient liquid phase (TLP) bonding of GTD-111 superalloy were investigated. The bonding process was applied using BNi-3 filler at temperatures of 1080, 1120, and 1160 °C for isothermal solidification time of 195, 135, and 90 min, respectively. Homogenization heat treatment was also applied to all of the joints. The results show that intermetallic and eutectic compounds such as Ni-rich borides, Ni−B−Si ternary compound and eutectic-γ continuously are formed in the joint region during cooling. By increasing t_J, intermetallic phases are firstly reduced and eventually eliminated and isothermal solidification is completed as well. With the increase of the holding time at all of the three bonding temperatures, the thickness of the athermally solidified zone (ASZ) and the volume fraction of precipitates in the bonding area decrease and the width of the diffusion affected zone (DAZ) increases. Similar results are also obtained by increasing T_J from 1080 to 1160 °C at t_J=90 min. Furthermore, increasing the T_J from 1080 to 1160 °C leads to the faster elimination of intermetallic phases from the ASZ. However, these phases are again observed in the joint region at 1180 °C. It is observed that by increasing the bonding temperature, the bonding width and the rate of dissolution of the base metal increase. Based on these results, increasing the homogenization time from 180 to 300 min leads to the elimination of boride precipitates in the DAZ and a high uniformity of the concentration of alloying elements in the joint region and the base metal.
Key words: TLP bonding joint; GTD-111 superalloy; isothermal solidification; microstructure; homogenization

1 Introduction

GTD-111 Ni-based superalloy as the modified version of IN-738 alloy was developed by General Electric in the 1970s and widely used in the gas turbines as the first stage blades [1,2]. Typically, GTD-111 turbine blades may experience a series of different damage phenomena during their services including thermal fatigue, wear, physical damages, high temperature corrosion and oxidation. Considering the high costs of remanufacturing of GTD-111 turbine blades, it will be more economical to have a clear perception of the methods of maintenance, repair and joining of this superalloy [3]. In this regard, it is necessary to recognize that the GTD-111 superalloy is a complex material in terms of the metallurgical and mechanical properties. So, it is difficult to make a joint similar to base metal for this superalloy.

Fusion welding, diffusion bonding and brazing are known as the main methods for repairing and/or bonding of different superalloys. Each of these methods has its own limitations. Non-equilibrium transformations in the fusion zone and interaction of the welding thermal cycle with strengthening

Corresponding author: Seyed Abdolkarim SAJJADI, Tel: +98-513-8817182, Fax: +98-513-8807182, E-mail: sajjadi@um.ac.ir
DOI: 10.1016/S1003-6326(21)65686-8

mechanisms of superalloys are the main sources of the formation of liquation cracking and poor weldability of Ni-based superalloys through fusion welding [4−6]. Diffusion bonding results in making the properties similar to the base metal; however, high pressure, long process time and costly equipment are usually required in this method [7,8]. Typically, borides and/or silicides are formed during the brazing process which in turn lead to the brittleness and degradation in the mechanical properties of the TLP bonding joints [9,10].

On the other hand, TLP bonding, as a hybrid process, benefits from both features of liquid phase bonding and diffusion bonding. This method, which can produce defect-free TLP bonding joints, has been known as an alternative for the conventional joining processes [11−23]. In this process, an alloying filler material (interlayer) containing melting point depressant (MPD) elements such as P, B, and Si is inserted between the surfaces to be bonded. Joining process is carried out at temperatures slightly higher than the liquidus temperature of interlayer. With diffusing MPD elements from interlayer to base metal, isothermal solidification begins from the joint/base metal interface and proceeds towards the centerline of joint region [24,25]. In general, TLP joining process is carried out in four steps: (1) heating base metal and interlayer just to melt the interlayer, (2) base metal dissolution, (3) isothermal solidification of liquid phase, and (4) homogenization of solid state [24,26]. After the completion of isothermal solidification, TLP-bonded joints become chemically more identical to their base metal through increasing the time and/or the temperature of homogenization heat treatment. In the TLP bonding process, completion of isothermal solidification and homogenization heat treatment are key steps to provide ideal joints [26]. This issue has been demonstrated by CAO et al [27].

As can be found in the literatures, joining time (t_J) and joining temperature (T_J) are the most important parameters in the TLP process. t_J is mainly dependent on the base metal system including phase diagram, diffusion coefficients, grain size, and some experimental parameters (such as interlayer thickness, joining pressure, and joining temperature) [28−30]. In ideal conditions, t_J should be optimized in a way which prevents the formation of brittle intermetallic phases and eventually guarantees a completion of isothermal solidification and formation of a single phase microstructure in the joint region [31]. Increasing the T_J leads to rising the rate of isothermal solidification and as a result declining the required time to complete the isothermal solidification (t_J). However, based on the microstructure stability of the base metal there is a critical temperature (T_J^*) that if $T_J>T_J^*$, the required time for completion of isothermal solidification increases [32−35]. Moreover, increasing the bonding temperature higher than the critical temperature has an opposite effects on the isothermal solidification time and the extent of secondary precipitate formation at the joint interface. It has been reported that B controls isothermal solidification process at 1100 and 1150 °C, while at bonding temperature of 1180 °C isothermal solidification is controlled by Ti atoms [34].

Despite previous research on TLP bonding process of superalloys, it is reasonable to make an ideal correlation between the microstructural effects of T_J and t_J in the TLP bonding process of GTD-111 Ni-based superalloy. For this reason, this research aims to evaluate the effects of T_J and t_J in the TLP bonding of GTD-111 superalloy. Moreover, to create an ideal joint, a homogenization treatment was applied on the samples joined under the optimum bonding conditions.

2 Experimental

In this investigation, standard cast GTD-111 Ni-based superalloy was used as the base material. Ni−Si−B (BNi-3) amorphous interlayer with a thickness of 38.0 μm was also applied as the filler material. The liquidus and solidus temperatures of interlayer were 1054 and 984 °C, respectively [36]. Table 1 shows the chemical composition of base metal and interlayer. The specimens with dimensions of 10 mm × 5 mm × 5 mm were prepared using an electrical discharge machine. To remove the oxide layers, joining surfaces were ground using 100, 220, 400, 600, and 800 emery papers and then ultrasonically cleaned in acetone for 15 min, sonicated in ethanol and immediately dried with hot air. After that, interlayer was inserted between two base metal specimens. To hold the sandwich assembly (GTD-111/BNi-3/GTD-111) and reduce metal flow during the TLP operation, a

Table 1 Chemical compositions of GTD-111 base metal and BNi-3 interlayer (wt.%)

Material	Ni	C	Cr	Co	Mo	Al	Ti	Si	Fe	Ta	B	W
GTD-111	Bal.	0.09	13.5	9.5	1.53	3.3	4.75	−	0.23	2.7	0.01	3.8
BNi-3	Bal.	0.06	−	−	−	−		4.5	−	−	3.2	−

Cr−Mo steel (DIN 1.4841) fixture was used (Fig. 1). In the TLP bonding process, due to the presence of liquid phase, no additional external pressure was applied during bonding. TLP bonding process was performed in a tube furnace at T_J=1080, 1120, 1160, and 1180 °C for different t_J under a vacuum of 1.33×10^{-3} Pa. Table 2 represents the values of t_J for each T_J. The samples were heated to T_J under a constant rate of 15 °C/min. After elapsing the t_J, the samples were furnace cooled. Finally, the TLP bonding joint isothermally solidified was homogenized at 1200 °C for 180, 240, and 300 min under vacuum of 1.33×10^{-3} Pa.

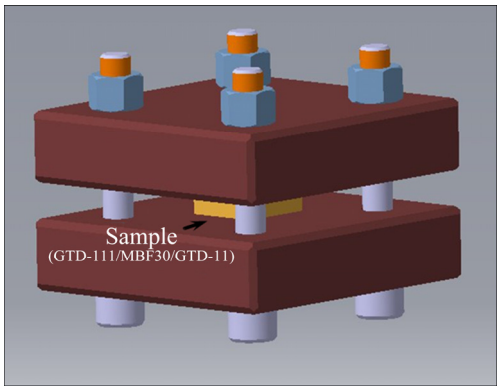

Fig. 1 3D schematic illustration of fixture used for joining process

Table 2 Values of T_J and t_J in TLP bonding processes

T_J/°C	t_J/min
1080	15, 90, 150, 165, 180, 195
1120	15, 45, 90, 105, 120, 135
1160	5, 15, 30, 45, 60, 75, 90
1180	90

TLP bonding processed samples were sectioned perpendicular to the join area and the cross-section of each specimen was ground to a final 2000# SiC paper and polished with 6, 3 and 1 μm water-based diamond suspensions (DP-Suspension P, Struers) to get a mirror-like surface. It should be mentioned that for each condition three samples were used. To reveal the microstructure, specimens were etched using Marble solution (10 g $CuSO_4$, 50 mL HCl, and 50 mL H_2O). To investigate the microstructure evolution, optical microscopy (OM) and scanning electron microscopy (SEM) (LEO−1450VP) equipped with energy dispersive X-ray spectroscopy (EDS), were applied. The width value of the joint zones was reported as an average of three measurements. To analyze the existing phases in the joint region, X-ray diffraction (XRD) technique was employed by a PANalytical diffractometer X-pert Pro with Cu K_α radiation (λ=1.54 Å) operating at 40 kV and 40 mA.

3 Results and discussion

3.1 Microstructure of base metal

Figure 2 represents a SEM image of the as-cast GTD-111 Ni-based superalloy. As can be seen, the microstructure consists of a γ-matrix (Ni solid solution) along with γ' precipitates [37], and some intragranular/intergranular carbides and $\gamma+\gamma'$ eutectic islands as well. The prevailing carbides which precipitate during solidification of GTD-111 are $M_{23}C_6$, $(Cr,Mo)_{23}C_6$, MC, and (Ta,W,Ti)C [38]. Distribution of $\gamma+\gamma'$ eutectic structure at serrated grain boundaries is due to the microsegregation of dissolved alloying elements at final stages of solidification [39].

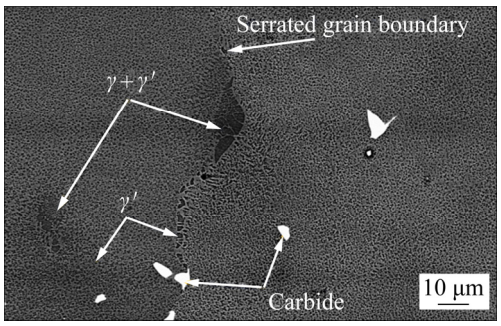

Fig. 2 Typical microstructure of as-received GTD-111 superalloy

3.2 Microstructural evolution in TLP bonding joint

Figure 3 shows the OM images of TLP bonding joint for T_J=1120 °C and t_J=15 min which

are typical microstructures of TLP bonding joints. Four distinct zones are observed: (1) isothermally solidified zone (ISZ), (2) athermally solidified zone (ASZ), (3) diffusion affected zone (DAZ) and (4) base metal (BM).

SEM images and chemical composition of the above-mentioned zones are shown in Fig. 4 and Table 3, respectively. As can be found, microstructure of Zone A consists of γ solid solution formed due to isothermal solidification. The base metal dissolution starts as the interlayer is melted. The phenomenon continues as long as a thermodynamic equilibrium between the base metal and liquid phase is established. Some boride precipitates are formed inside the joint region, mainly adjacent to the joint interface (boride zone in Fig. 4(a)) and Region E in Fig. 4(b)). These precipitates are Ni-rich according to Table 3. This region has rarely been reported in any previous work on similar alloys. Researches on TLP bonding joints of Ni−Ni/Ni−B−Si/Ni−Al have confirmed that the diffusion of B from interlayer into the BM, during the heating and melting interlayer, was the reason for the occurrence of this zone [14]. At joining temperatures, interlayer is melted and MPD elements such as B and Si diffuse from the interlayer to the base metal and concentration of alloying elements (e.g. Cr) in the liquid phase increases; consequently, liquidus temperature of the molten interlayer increases [40]. As the liquidus

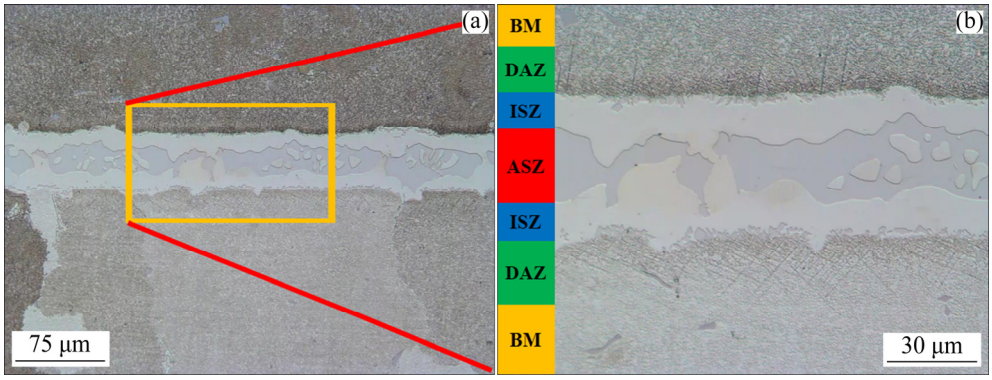

Fig. 3 Optical micrographs of sample TLP-bonded at 1120 °C for 15 min: (a) General view of joint region; (b) Higher magnification of specified region in (a)

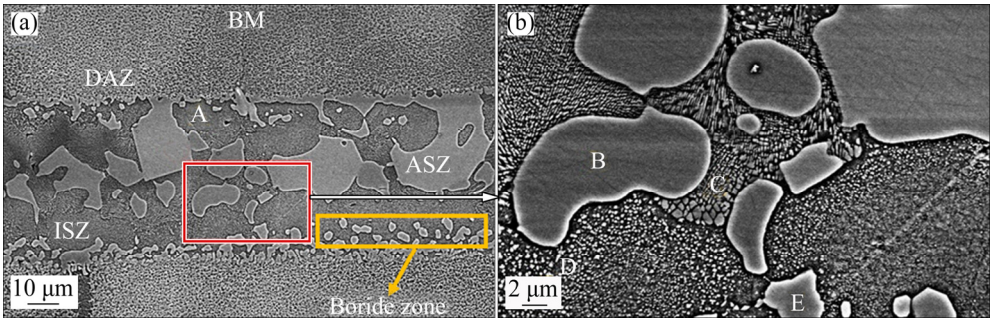

Fig. 4 Cross-sectional SEM images of sample TLP-bonded at 1120 °C for 15 min: (a) Overview image of joint; (b) Higher magnification of region specified in (a)

Table 3 Typical SEM/EDS analysis results of regions specified in Fig. 4 (wt.%)

Region	Ni	Cr	Al	Ti	Co	Fe	W	Mo	Others
A in Fig. 4(a)	87.94	4.38	0.76	0.98	2.46	N/A	N/A	N/A	3.48
B in Fig. 4(b)	86.29	2.94	1.89	4.84	2.88	N/A	N/A	N/A	1.16
C in Fig. 4(b)	82.82	2.1	1.05	N/A	N/A	N/A	N/A	N/A	14.03
D in Fig. 4(b)	81.89	3.02	1.91	N/A	1.34	N/A	N/A	N/A	11.84
E in Fig. 4(b)	85.79	3.62	1.11	5.21	3.3	N/A	N/A	N/A	0.97

N/A: Mass fraction of element is less than the detection limit

temperature reaches the joining temperature, isothermal solidification begins (from the interlayer/base metal interface) and proceeds towards the joint center. The presence of some alloying elements such as Cr, Co, Al, and Ti which were not present in the initial composition of BNi-3 reveals the base metal dissolution. Because of the absorption of the excited X-rays of light elements and as a result of EDS limitations, B was not detected in the ISZ. On the other hand, due to lower diffusion rate of Si and its higher solubility limit compared with B [41], it can accumulate in this region (Table 3).

When isothermal solidification is not completed, undesirable phases are formed in the middle of the joint (ASZ zone) during the cooling from the bonding temperature. According to Fig. 4(b), Table 3 and previous works [14,31,42], ASZ is formed due to the lack of enough time for the completion of isothermal solidification during the cooling from joining temperature. Boride precipitates in the ASZ zone are formed in two parts of the joint: centerline and the inner areas adjacent to the interface (Fig. 4). The ASZ region consists of Ni-rich boride phases (Region B), Ni−Si−B ternary component (Region C), and eutectic γ (Region D). The microstructure evolution of ASZ is mainly governed by segregation of solute elements during athermal solidification [43]. The solidification path depends on the relative redistribution behavior of each solute in the system [43]. During formation and growth of the dendrites, some alloying elements e.g. Ti, Si and Al, segregate towards the remaining liquid phase and consequently, reduce the liquidus temperature [44].

This process, known as "constitutional super-cooling", has been already discussed by ASSADI et al [45] and SHENG et al [46]. Considering low segregation coefficient of B in Ni−B hypoeutectic alloys (8×10^{-3}) and its low solubility in γ matrix [47], this element has also affinity to segregate in the remaining liquid. As a result, after reaching the solubility limits of segregated elements in austenitic γ, Ni-rich boride phases gradually appear in the ASZ (Region B in Table 3). According to the solidification behavior and microstructural evolution of ASZ, B is the most effective alloying element in isothermal solidification. In general, low solubility of B in γ-Ni and its extremely low segregation coefficient compared to the Si are the main factors for the latter reasoning [31]. It has been reported that very low solubility of B in Ni and partition coefficient of B in Ni lead to rejection of B into the adjacent melt shifting composition of melt towards the eutectic composition. Thus, with progressing of solidification, binary eutectic of γ-solid solution and Ni-boride is formed [34]. Considering the Si concentration in the MBF 30 (before melting), very low amount of Si in the Ni-rich boride phase (i.e. Si has segregated in the adjacent liquid), and Ni-enrichment of Region C (Table 3), it is concluded that Si has segregated into the remaining liquid phase. Ni−Si−B compounds might be formed in Region C as a result of combination of Si and B in the existing liquid. As reported by POURANVARI et al [41], this phase is Ni_6Si_2B for the TLP process of IN718.

The eutectic γ (Region D) consisting of very fine nickel−silicide precipitates dispersed in γ-nickel matrix is also formed. The exact amount of Si in these eutectic precipitates cannot be determined; however, EDS results (Region D in Table 3) clearly demonstrate the large amounts of Si in Region D. According to the Ni−Si phase diagram [44] and Si concentration of the fine precipitates (~8 wt.%), Ni_3Si might be stable in Region D. Solubility limit of Si in γ-Ni at 1120 °C and room temperature is 7.8 and 4 wt.%, respectively. This significant reduction in the solubility limit along with the fine morphology of silicide precipitates indicate that the Ni_3Si most probably is formed from the Si-rich γ solid solution during cooling. The presence of these silicide phases has been reported by other researchers [34,38].

Figure 5 represents the typical SEM images/ XRD pattern of the DAZ in the base metal/joint interface. The boride phases identified by XRD are mainly Ni_3B and CrB (Fig. 5(e)). EDS analysis result of the boride precipitates is given in Table 4. These borides are not present at large distances from the joint/BM interface. As can be seen, in spite of isothermal solidification which in turn prevents the formation of brittle intermetallic phases at the center of joint (ASZ-free), secondary precipitates with blocky and needle-like morphologies are formed even up to 30 μm inside the base metal in the DAZ. Observation of such precipitates has been reported by many researchers [14,31]. GALE and WALLACH [40] showed that boride precipitates in

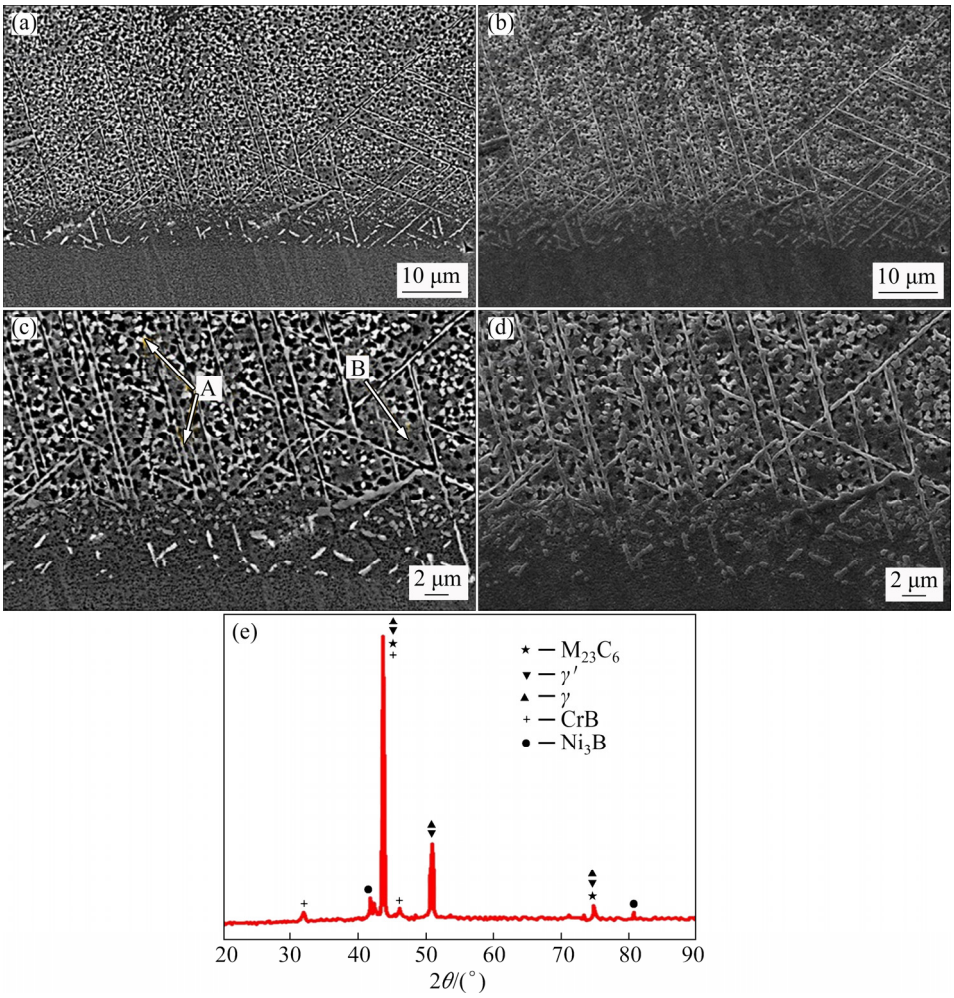

Fig. 5 SEM images (a−d) and XRD pattern (e) of DAZ in base metal/joint interface under T_J=1120 °C and t_J=15 min condition: (a, c) Back-scattered electron (BS) images; (b, d) Secondary electron (SE) images

Table 4 Typical SEM/EDS analysis results of positions specified in Fig. 5 (wt.%)

Position	Ni	Cr	Al	Ti	Co	Fe	W	Mo	Si
A	57.66	16.42	4.52	6.56	7.84	N/A	N/A	4.82	2.18
B	67.7	10.74	3.51	7.2	8.78	N/A	N/A	N/A	2.07

N/A: Mass fraction of element is less than the detection limit

this region (DAZ) are formed during holding at the bonding temperature, not during the cooling to room temperature. Due to limited diffusion of B towards the base metal, density of these phases decreases from the base metal/joint interface to the base metal gradually (Figs. 5(a, b)). The morphology of these fine precipitates suggests that they are most probably formed through a precipitation reaction in solid state. It should also be considered due to small distances of diffusion for these types of reactions, fine precipitates are not observed at distances far from the base metal/joint interface. In fact, very low solubility of B in γ-Ni [47], its high diffusivity compared to the Si [41], and the presence of Cr and Mo in the matrix which are strong boride formers, can be considered as the main reasons of formation of boride precipitates [13,34,41]. EDS results of these precipitates (Table 4, Position A) also demonstrate that they are enriched in Cr and Mo. Two mechanisms have been reported for the formation of these boride precipitates: (1) solid-state diffusion of B in the base metal before the completion of base metal dissolution and (2) solid-state diffusion of B in the base metal during the isothermal solidification [34,40].

Study of formation of boride precipitates in the current research indicates that the precipitates are formed in the substrate (DAZ) during holding at the bonding temperature once the solubility of boron in the substrate has been exceeded. Therefore, both mechanisms are likely operating (e.g. diffusion of B can occur during the base metal dissolution and/or during the isothermal solidification).

In general, the formation of (Cr,Mo)-rich boride precipitates in the DAZ has negative effects on the high temperature performance and corrosion resistance of the joint because of depletion of base metal from the beneficial elements such as Cr and Mo [14,41]. Moreover, the brittle nature of the boride phases can be the other reason for decreasing mechanical properties.

Silicide phases, unlike borides, are not formed in DAZ due to the low diffusivity of Si in γ-Ni. It should be mentioned that the diffusion coefficient of Si in Ni (3.09×10^{-14} m^2/s at 1100 °C) is much lower than that of B in Ni (6.22×10^{-11} m^2/s at 1100 °C). Moreover, the solubility limit of Si in Ni-base matrix is higher than that of B [41]. The other factor preventing the formation of silicide phases is the lack of Cr and Mo atoms because they are already tied up in the boride phases.

3.3 Joining parameters and microstructure of TLP bonding joints

3.3.1 Time

The microstructures of the joints at T_J=1120 °C for t_J=15, 45, 90, 120, and 135 min are shown in Figs. 6(a−e), respectively. The continuity and thickness of the eutectic structure in the ASZ are

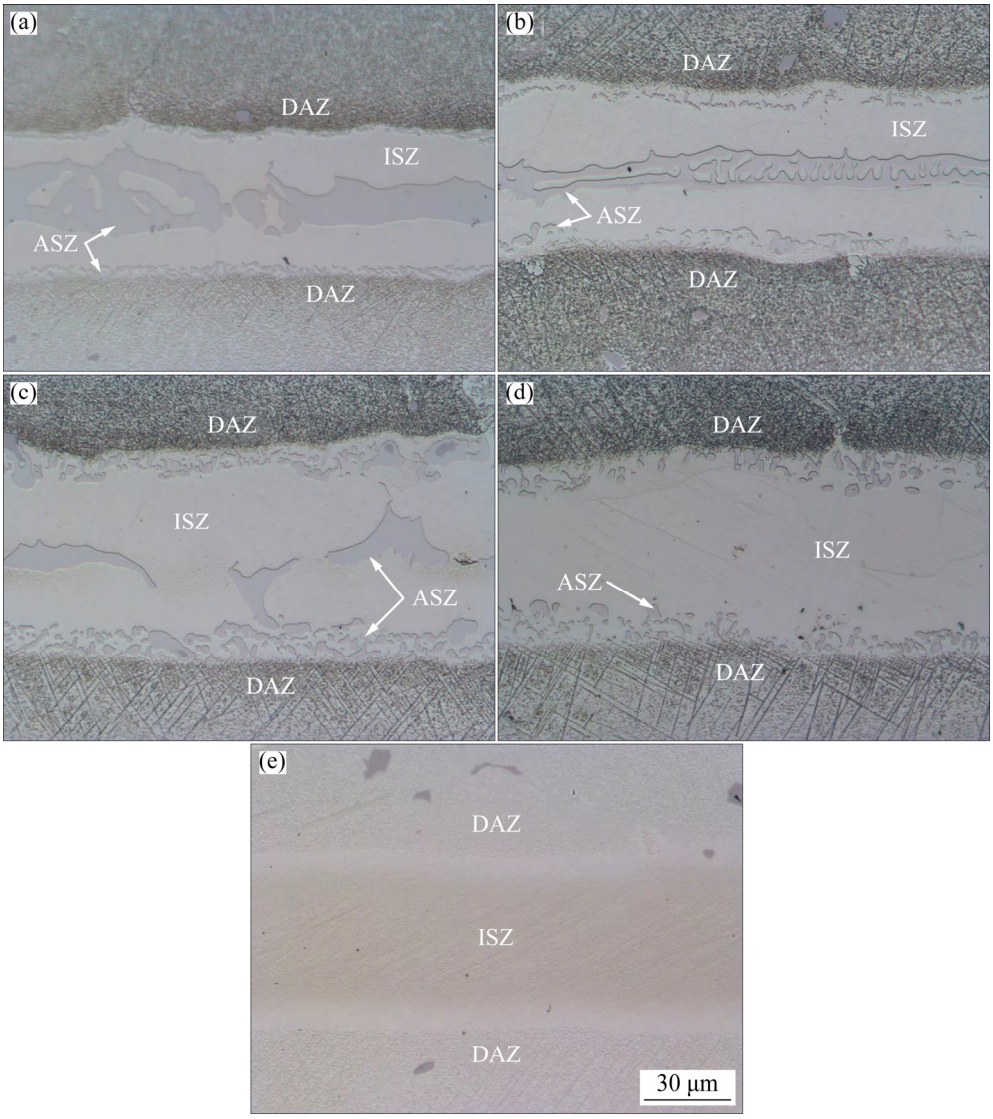

Fig. 6 Typical metallographic images of TLP bonding joints produced at 1120 °C for different time: (a) 15 min; (b) 45 min; (c) 90 min; (d) 120 min; (e) 135 min

reduced with increasing bonding time [14]. In addition, the extent of the isothermally solidified liquid and as a result the width of the ISZ increases drastically. The reason for this is the increased diffusion of MPD alloying elements, especially B, from the interlayer into the BM. The precipitates are completely removed from joint region and a complete isothermally solidified joint can be seen after 135 min holding time at 1120 °C (Fig. 6(e)). Variation of width of ASZ with t_J for different T_J is also indicated in Fig. 7. As can be seen, the ASZ size decreases with increasing bonding temperature and bonding time due to more diffusion of melting point depressant (MPD) elements into the base metal. When t_J reaches 135 min, eutectic phases are not observed in the joint region (Figs. 6(e) and 7). Therefore, it is realized that T_J=1120 °C and t_J= 135 min are the optimum conditions for achieving a complete isothermal solidification.

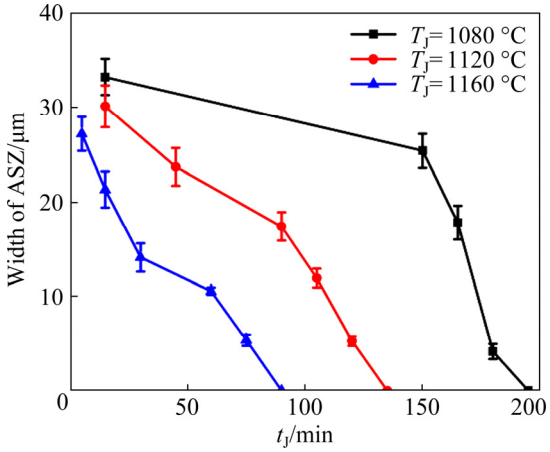

Fig. 7 Variation of width of ASZ with t_J at different T_J

Figure 8 depicts the SEM image and corresponding EDS elemental spectra of a eutectic phase-free joint produced at T_J=1120 °C and t_J=135 min, which reveals that the isothermal solidification is completed and a single solid solution phase has been obtained. According to the EDS spectra in Fig. 8, higher contents of Ni and Si at the middle of joint compared with the base metal are due to the presence of these elements in the interlayer. On the other hand, the presence of alloying elements such as Cr, Ti, and Al proves the diffusion of these elements from the base metal to the interlayer (i.e. dissolution of the base metal).

The variation of the width of DAZ with t_J at different T_J is shown in Fig. 9. Size and distribution of these precipitates depend on the bonding time

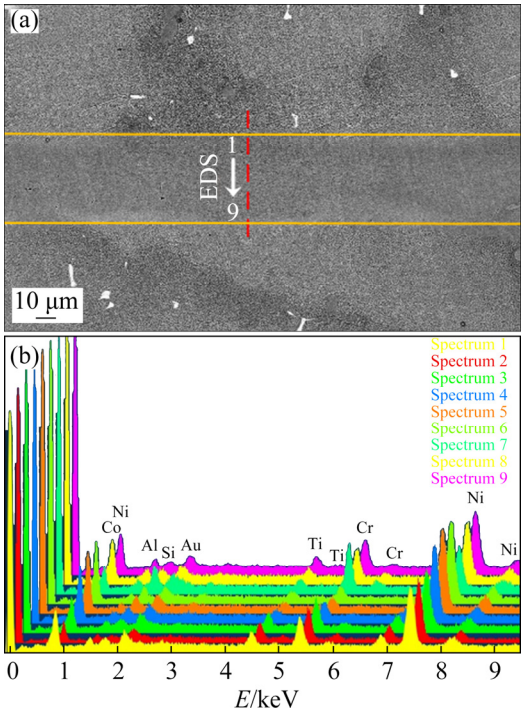

Fig. 8 SEM image of TLP bonding joint produced at 1120 °C and 135 min conditions along with corresponding EDS analysis result

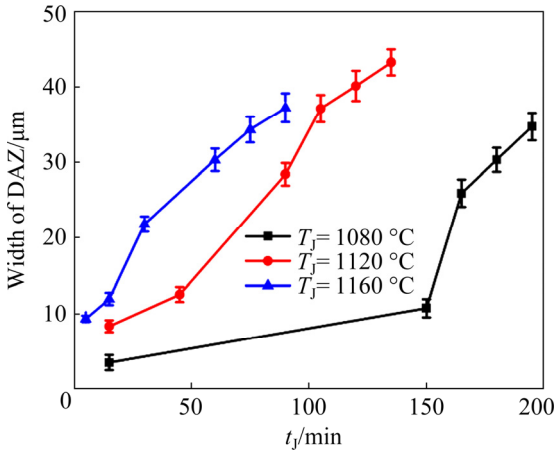

Fig. 9 Variation of width of DAZ with t_J at different T_J

and temperature. As can be seen in Fig. 9, and also as stated in literature, area of formation of the secondary precipitates at DAZ increases with time increment [48]. As seen, with increasing the t_J from 15 to 135 min at 1120 °C, the width of DAZ increases from (8.2±0.6) to (43.1±0.8) μm. Such increases can also be observed at 1080 and 1160 °C. Enhanced effective diffusion of B into the base metal can be considered as the main reason of the increase in width of DAZ [49]. From Fig. 6, as a typical microstructure of DAZ, by moving away from the base metal/joint interface to the base metal,

the morphology of boride precipitates in the DAZ varies from blocky shaped to needle-like. This change in morphology is mainly due to the internal strains associated with the solid-state transformation [50,51]. Due to the presence of large stresses in the vicinity of base metal/joint interface, blocky shaped precipitates tend to occur in this region. By moving away from the joint metal/joint interface, stress values and their effects on the morphology of precipitates decrease and consequently needle-like morphology will be more stable [50,51]. In addition, by increasing the t_J, more stresses will be relieved and the volume fraction of needle-like precipitates will be increased.

3.3.2 Temperature

In general, the rate of isothermal solidification substantially depends upon T_J and diffusibility of MPD elements. To study the effect of T_J on the microstructural evolution of joint, TLP bonding process was performed at 1080−1180 °C for t_J=90 min (Fig. 10). Increasing the temperature from 1080 to 1160 °C results in decreasing thickness and continuity of intermetallic phases in the joint region. This phenomenon occurs due to the increasing diffusion of MPD elements from joint district to the base metal, which leads to a higher rate of isothermal solidification. At T_J=1160 °C, isothermal solidification is eventually completed and a joint with no intermetallic phases is obtained (Fig. 10(c)). So, it can be stated that MPD elements (especially B) determine the rate of isothermal solidification and microstructural evolutions in the joint region. It is worth noting that the required time for complete diffusion of B into the base metal (i.e. completion of isothermal solidification) significantly decreases as the temperature increases from 1080 to 1160 °C (as shown in Fig. 7).

By increasing the T_J to 1180 °C (t_J=90 min), the eutectic phases unexpectedly appear in the center of join region (Fig. 10(d)). Two phenomena can be considered as the main reasons of this fact: (1) At T_J=1180 °C, base metal dissolution and diffusion of its constituents (especially Ti) into the liquid phase are considerable. (2) Increasing T_J to values more than the eutectic temperature severely reduces the solubility limit of B in γ-Ni [47] and consequently, leads to B segregation into the liquid phase. As a result, liquid phase enriches in Ti and B, the liquidus temperature decreases, and consequently required time for completion of the isothermal solidification increases. This argument is

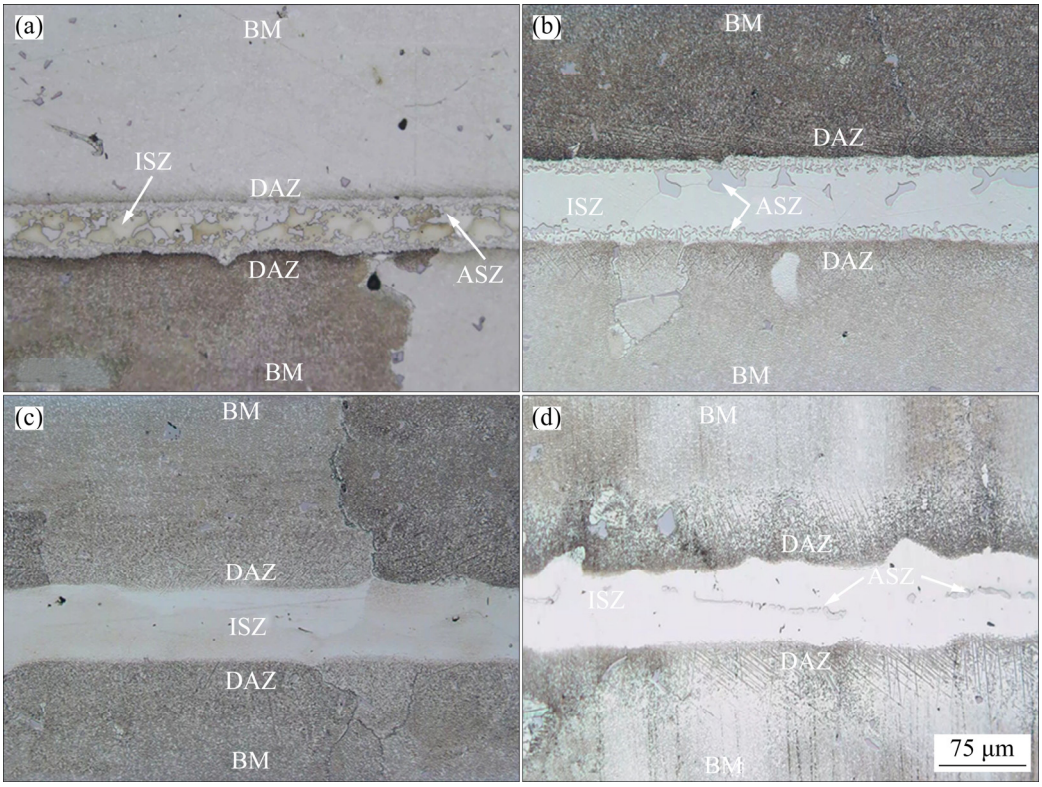

Fig. 10 Optical microscopy images of TLP bonding joints produced at different temperatures (t_J=90 min): (a) 1080 °C; (b) 1120 °C; (c) 1160 °C; (d) 1180 °C

in agreement with the results obtained by JALILVAND et al [52]. The critical temperature of the GTD-111 TLP bonding joints is 1160 °C, which is consistent with the results of POURANVARI et al [34]. In fact, the rate of isothermal solidification at 1080−1180 °C is determined by the diffusion of MPD elements (namely B) and alloying elements of the base metal (namely Ti), respectively. Generally speaking, B element can affect the rate of isothermal solidification by two ways: (1) Segregation of B in the remained liquid phase in the joint region due to low solubility of B in γ-Ni [47], which decreases the rate of isothermal solidification. (2) Higher diffusibility of B compared to Si (according to Ni−B and Ni−Si binary phase diagrams [47]) results in the diffusion of B from joint region to the base metal and declining the volume fraction of the remnant liquid in this area and also development of ISZ with increasing bonding time and temperature.

From Fig. 9, it can also be deduced that by increasing the t_J, the width of DAZ increases. This can be directly attributed to the increase in the diffusibility of MPD elements (namely B) into the base metal with temperature.

3.4 Homogenization treatment

Figure 11 presents the OM images of joints made at 1120 °C for 135 min (i.e. an isothermally solidified joint), and then homogenized at 1200 °C for 180, 240, and 300 min. Moreover, Fig. 12 shows the SEM microstructure of joint sample homogenized at 1200 °C for 300 min. As can be seen from Figs. 11 and 12, as the homogenization time elapses, boride phases in DAZ are gradually eliminated, and the microstructural features of the joint become closer to the base metal. Due to the enhanced diffusion of alloying elements from the base metals to the joint, a uniform redistribution of alloying elements has been achieved in the joint region after the homogenization treatment. However, there is not any evidence of gamma prime precipitates in the joint region. This can be attributed to the low amounts of gamma prime forming elements such as Ti and Al in this area (Fig. 12) [53]. As reported by AMIRI et al [14], POURANVARI et al [54] and ASADI et al [55], higher concentration of alloying elements in the joint region is accompanied by solid solution strengthening in ISZ.

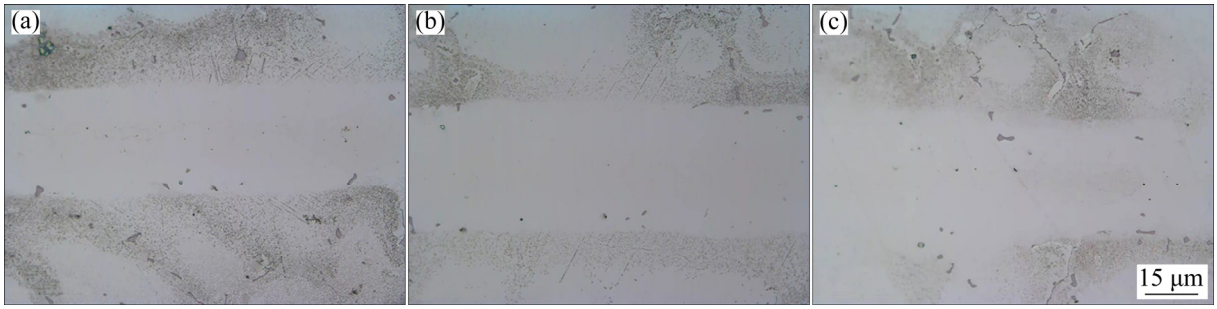

Fig. 11 Optical microscopy images of TLP bonding joints produced at 1120 °C for 135 min and then homogenized at 1200 °C for different time: (a) 180 min; (b) 240 min; (c) 300 min

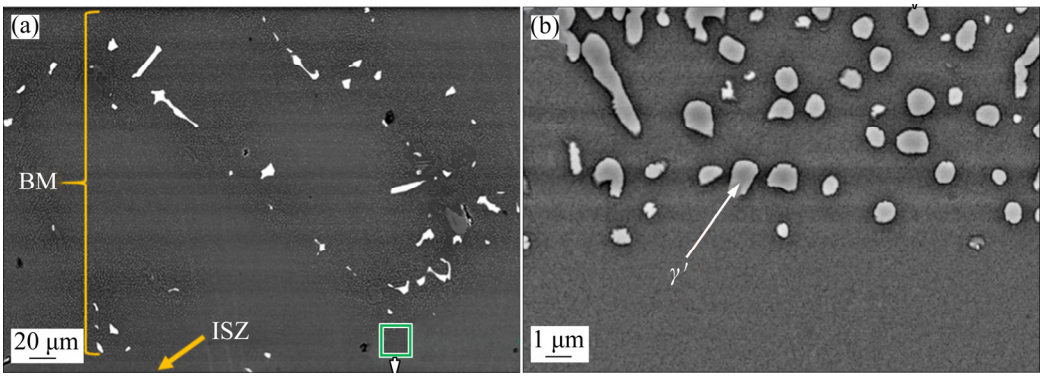

Fig. 12 SEM images of TLP bonding joint after homogenization at 1200 °C for 300 min (The TLP bonding joint was produced at 1120 °C for 135 min)

4 Conclusions

(1) The joining processes under T_J=1080 °C and t_J<200 min, T_J=1120 °C and t_J<135 min, and T_J=1160 °C and t_J<90 min conditions lead to the incomplete isothermal solidification and formation of intermetallics, Ni-rich borides, and eutectic phases in ASZ of the TLP bonding joint region.

(2) Boride phases enriched in Cr and Mo are formed as blocky and needle-like morphologies in DAZ.

(3) By increasing t_J (at constant T_J), thickness and continuity of eutectic phases existing in ASZ gradually decrease and width of ISZ significantly increases, and eventually no eutectic phase is observed in ASZ.

(4) By increasing t_J (at constant T_J), width of DAZ increases and by moving away from joint region towards the base metal, the morphology of boride precipitates in this region is changed from blocky to needle-like.

(5) Increasing the T_J from 1080 to 1160 °C (at constant t_J), increases the rate of isothermal solidification, and consequently reduces the thickness and continuity of intermetallic phases in the joint center. At T_J=1160 °C and t_J=90 min, isothermal solidification is completed. Moreover, increasing the T_J leads to the development of DAZ.

(6) As the bonding temperature increases above the critical temperature of GTD-111 TLP bonding joint (1160 °C), eutectic phases and intermetallic compounds are formed again in the bonding region.

(7) Subsequent homogenization treatment increases the possibility of producing ideal joints with minimum boride phases in DAZ and microstructural features similar to the base metal.

Acknowledgments

The authors appreciate the support from Ferdowsi University of Mashhad (FUM), Iran, under the research scheme No. 3/39728. The authors also thank MAPNA Turbine Blade Engineering & Manufacturing Company-Parto for providing the materials used in this work.

References

[1] DALEO J A, WILSON J R. GTD111 alloy material study [C]//Proc InTurbo Expo 1996. Birmingham, PA: GT, 1996: V005T12A017.

[2] BOYCE M P. Gas turbine engineering handbook [M]. Fourth ed. Oxford: Elsevier, 2011.

[3] HUANG X, MIGLIETTI W. Wide gap braze repair of gas turbine blades and vanes−A review [J]. Journal of Engineering for Gas Turbines and Power, 2012, 134: 010801.

[4] SCHIRRA J J, CALESS R H, HATALA R W. The effect of Laves phase on the mechanical properties of wrought and cast + HIP Inconel 718 [J]. Superalloys, 1991: 375–388.

[5] JANAKI RAM G D, VENUGOPA REDDY A, PRASAD RAO K, MADHUSUDHAN REDDY G. Control of laves phase in Inconel 718 GTA welds with current pulsing [J]. Science and Technology of Welding and Joining, 2004, 9(5): 390−398.

[6] XU J J, ZHAO Y F, GUO P F, WEN X L, LI Q G, YANG H O, DONG H B, XUE L, HUANG W D. HAZ liquation cracking mechanism of IN-738LC superalloy prepared by laser solid forming [J]. Metallurgical and Materials Transactions A, 2018, 49: 5118−5136

[7] SHIRZADI A A, WALLACH E R. New method to diffusion bond superalloys [J]. Science and Technology of Welding and Joining, 2004, 9: 37–40.

[8] MACDONALD W D, EAGAR T W. Transient liquid phase bonding [J]. Annual Review of Material Science, 1992, 22(1): 23–46.

[9] TUNG S K, LIM L C, LAI M O. Microstructural evolution and control in BNi-4 brazed joints of nickel 270 [J]. Scripta Metallurgica et Materialia, 1995, 33(8): 1253–1259.

[10] TUNG S K, LIM L C, LAI M O. Solidification phenomena in nickel base brazes containing boron and silicon [J]. Scripta Materialia, 1996, 34(5): 763–769.

[11] NICHOLAS M G. The brazing of ceramics: Material science aspect of reactive braze alloys [M]//NATO ASI Series 3. Vol. 58. Springer, Dordrecht, 1998: 97–109. DOI:10.1007/978-94-017-1917-9-9.

[12] PAULONIS D F, DUVALL D S, OWCZARSKI W A. Diffusion bonding utilizing transient liquid phase [P]. US Potent US 3678570. 1972−07−25.

[13] SHAMSABADI A Y, BAKHTIARI R. TLP bonding of IN738/MBF20/IN718 system [J]. Journal of Alloys and Compounds, 2016, 685: 896–904.

[14] AMIRI D, SAJJADI S A, BAKHTIARI R, KAMYABI-GOL A. The role of TLP process variables in improvement of microstructure and mechanical properties in TLP joints of GTD-111/Ni−Cr−Fe−B−Si/GTD-111 system [J]. Journal of Manufacturing Processes, 2018, 32: 644−655.

[15] MALEKI V, OMIDVAR H, RAHIMIPOUR M. Effect of gap size on microstructure of transient liquid phase bonded IN-738LC superalloy [J]. Transactions of Nonferrous Metals Society of China, 2016, 26(2): 437−447.

[16] YAN G, BHOWMIK A, NAGARAJAN B, SONG X, SUNG C T, MING J T. Bonding temperature effects on the wide gap transient liquid phase bonding of Inconel 718 using BNi-2 paste filler metal [J]. Applied Surface Science, 2019, 484: 1223−1233.

[17] GHASEMI A, POURANVARI M. Thermal processing strategies enabling boride dissolution and gamma prime precipitation in dissimilar nickel-based superalloys transient liquid phase bond [J]. Materials & Design, 2019, 182:

108008.

[18] HADIBEYK S, BEIDOKHTI B, SAJJADI S A. Effect of bonding time and homogenization heat treatment on the microstructure and mechanical properties of the transient liquid phase bonded dissimilar GTD-111/FSX-414 TLP superalloys [J]. Journal of Alloys and Compounds, 2018, 731: 929−935.

[19] BRIDGES D, XU R, HU A. Microstructure and mechanical properties of Ni nanoparticle-bonded Inconel 718 [J]. Materials & Design, 2019, 174: 107784.

[20] MALEKAN A, FARVIZI M, MIRSALEHI S E, SAITO N, NAKASHIMA K. Influence of bonding time on the transient liquid phase bonding behavior of hastelloy X using Ni−Cr−B−Si−Fe filler alloy [J]. Materials Science and Engineering A, 2019, 755: 37−49.

[21] LIU M, SHENG G, HE H, JIAO Y. Microstructural evolution and mechanical properties of TLP bonded joints of Mar-M247 superalloys with Ni−Cr−Co−W−Ta−B interlayer [J]. Journal of Materials Processing Technology, 2017, 246: 245−251.

[22] BAKHTIARI R. Effect of configuration and composition of interlayer on TLP joints of FSX-414 superalloy [J]. Journal of Materials Processing Technology, 2016, 231: 8−17.

[23] POURANVARI M, EKRAMI A, KOKABI A H. Role of base-metal composition in isothermal solidification during diffusion brazing of nickel-based superalloys [J]. Science and Technology of Welding and Joining, 2018, 23: 13−18.

[24] PAULONIS D F, DUVALL D S, OWCZARSKI W A. Diffusion bonding utilizing transient liquid phase: United States Patent, 3678 570 [P]. 1972−07−25.

[25] COOK G O, SORENSEN C D. Overview of transient liquid phase and partial transient liquid phase bonding [J]. Journal of Materials Science, 2011, 46(16): 5305−5323.

[26] GALE W F, BUTTS D A. Transient liquid phase bonding [J]. Science and Technology of Welding and Joining, 2004, 9(4): 283−300.

[27] CAO J, WANG Y F, SONG X G, LI C, FENG J C. Effects of post-weld heat treatment on microstructure and mechanical properties of TLP bonded Inconel 718 superalloy [J]. Materials Science and Engineering A, 2014, 590: 1−6.

[28] PADRON T, KHAN T I, KABIR M J. Modelling the transient liquid phase bonding behaviour of a duplex stainless steel using copper interlayers [J]. Materials Science and Engineering A, 2004, 385: 220−228.

[29] MACDONALD W D, EAGAR T W. Isothermal solidification kinetics of diffusion brazing [J]. Metallurgical and Materials Transactions A, 1998, 29: 315−325.

[30] ZHOU Y, NORTH T H. Kinetic modelling of diffusion-controlled, two-phase moving interface problems [J]. Modelling and Simulation in Materials Science and Engineering, 1993, 1(4): 505−516.

[31] POURANVARI M, EKRAMI A, KOKABI A H. Microstructure development during transient liquid phase bonding of GTD-111 nickel-based superalloy [J]. Journal of Alloys and Compounds, 2008, 461: 641−647.

[32] SCHNELL A, STANKOWSKI A, MARCOS E. A study of the diffusion brazing process applied to the single crystal superalloy CMSX-4 [C]//Proc ASME Turbo Expo 2006. Barcelona, PA: GT, 2006: 949−961.

[33] OJO O A, RICHARDS N L, CHATURVEDI M C. Isothermal solidification during transient liquid phase bonding of Inconel 738 superalloy [J]. Science and Technology of Welding and Joining, 2004, 9(6): 532−540.

[34] POURANVARI M, EKRAMI A, KOKABI A H. Effect of bonding temperature on microstructure development during TLP bonding of a nickel base superalloy [J]. Journal of Alloys and Compounds, 2009, 469: 270−275.

[35] BAKHTIARI R, EKRAMI A, KHAN T I. The effect of TLP bonding temperature on microstructural and mechanical property of joints made using FSX-414 superalloy [J]. Materials Science and Engineering A, 2012, 546: 291−300.

[36] RABINKIN A. Brazing with (NiCoCr)−B−Si amorphous brazing filler metals: Alloys, processing, joint structure, properties, applications [J]. Science and Technology of Welding and Joining, 2004, 9(3): 181−199.

[37] DAVYDOV D, KAZANTSEVA N, VINOGRADOVA N, STEPANOVA N N. Analysis of the grain boundary microstructure and degradation in a gas turbine blade [C]// Scientific Proceedings III International Scientific Conference “Materials Science. Non-Equilibrium Phase Transformations”, 2017: 26−29.

[38] SAJJADI S A, NATEGH S, GUTHRIE R I L. Study of microstructure and mechanical properties of high performance Ni-base superalloy GTD-111 [J]. Materials Science and Engineering A, 2002, 325: 484−489.

[39] HOFFELNER W, KNY L E, STICKLER R, MCCALL W J. Effects of aging treatments on the microstructure of the Ni-base superalloy IN−738 [J]. Materialwissenschaft und Werkstofftechnik, 1979, 10(3): 84−92.

[40] GALE W F, WALLACH E R. Microstructural development in transient liquid-phase bonding [J]. Metallurgical Transactions A, 1991, 22(10): 2451−2457.

[41] POURANVARI M, EKRAMI A, KOKABI A H. Solidification and solid state phenomena during TLP bonding of IN718 superalloy using Ni–Si–B ternary filler alloy [J]. Journal of Alloys and Compounds, 2013, 563: 143−149.

[42] POURANVARI M, EKRAMI A, KOKABI A H. Diffusion induced isothermal solidification during transient liquid phase bonding of cast IN718 superalloy [J]. Canadian Metallurgical Quarterly, 2014, 53(1): 38−46.

[43] POURANVARI M, EKRAMI A, KOKABI A H. Phase transformations during diffusion brazing of IN718/Ni−Cr−B/IN718 [J]. Materials Science and Technology, 2013, 29(8): 980−984.

[44] SUNG P K, POIRIER D R. Liquid−solid partition ratios in nickel-base alloys [J]. Metallurgical and Materials Transactions A, 1999, 30(8): 2173−2181.

[45] ASSADI H, SHIRZADI A A, WALLACH E R. Transient liquid phase diffusion bonding under a temperature gradient: Modelling of the interface morphology [J]. Acta Materialia, 2001, 49(1): 31−39.

[46] SHENG N C, LIU J D, JIN T, SUN X F, HU Z Q. Wide gap TLP bonding a single-crystal superalloy: Evolution of the L/S interface morphology and formation of the isolated grain boundaries [J]. Metallurgical and Materials Transactions A, 2013, 44(4): 1793−1804.

[47] TOKUNAGA T, NISHIO K, HASEBE M. Thermodynamic

study of phase equilibria in the Ni−Si−B system [J]. Journal of Phase Equilibria, 2001, 22(3): 291.

[48] BINESH B, GHAREHBAGH A J. Transient liquid phase bonding of IN738LC/MBF-15/IN738LC: Solidification behavior and mechanical properties [J]. Journal of Materials Science and Technology, 2016, 32(11): 1137−1151.

[49] KHAKIAN M, NATEGH S, MIRDAMADI S. Effect of bonding time on the microstructure and isothermal solidification completion during transient liquid phase bonding of dissimilar nickel-based superalloys IN738LC and Nimonic 75 [J]. Journal of Alloys and Compounds, 2015, 653: 386−394.

[50] LIU J D, JIN T, ZHAO N R, WANG Z H, SUN X F, GUAN H R, HU Z Q. Study of Ni–Cr–Co–W–Mo–B interlayer alloy and its bonding behaviour for a Ni-base single crystal superalloy [J]. Scripta Materialia, 2003, 48(9): 1283−1288.

[51] LIU J D, JIN T, ZHAO N R, WANG Z H, SUN X F, GUAN H R, HU Z Q. Effect of temperature on formation of borides in TLP joint of a kind of nickel-base single crystal superalloy [J]. Materials Science Forum, 2007, 546: 1245−1248.

[52] JALILVAND V, OMIDVAR H, RAHIMIPOUR M R, SHAKERI H R. Influence of bonding variables on transient liquid phase bonding behavior of nickel based superalloy IN-738LC [J]. Materials & Design, 2013, 52: 36−46.

[53] AMIRI D, SAJJADI S A, KAMYABI-GOL A. Pre- and post-TLP bond solution treatments: Effects on the microstructure and mechanical properties of GTD-111 superalloy [J]. Journal of Manufacturing Processes, 2020, 57: 36−47.

[54] POURANVARI M, EKRAMI A, KOKABI A H. TLP bonding of cast IN718 nickel based superalloy: Process–microstructure–strength characteristics [J]. Materials Science and Engineering A, 2013, 568: 76−82.

[55] ASADI J, SAJJADI S A, OMIDVAR H. Creep properties of Ni-based superalloy GTD-111 joints produced by transient liquid phase method using BNi-3 filler [J]. Journal of Manufacturing Processes, 2020, 58: 1103−1114.

GTD-111 高温合金瞬时液相连接过程中显微组织的变化

Javad ASADI[1], Seyed Abdolkarim SAJJADI[1], Hamid OMIDVAR[2]

1. Materials and Metallurgical Engineering Department, Faculty of Engineering,
Ferdowsi University of Mashhad, Mashhad, Iran;
2. Department of Materials and Metallurgical Engineering,
Amirkabir University of Technology (Tehran Polytechnic), Tehran, Iran

摘　要：研究连接温度和时间对瞬时液相连接 GTD-111 高温合金显微组织的影响。连接过程采用 BNi-3 填料，在 1080、1120 和 1160 °C 下，分别进行 195、135 和 90 min 的等温凝固，再进行均匀化热处理。结果表明，在冷却过程中，接头区域连续形成富 Ni 硼化物、Ni−B−Si 三元化合物和共晶 γ 的金属间化合物和共晶化合物。随着连接时间的延长，金属间化合物相首先减少，最终被消除，等温凝固完成。三种温度下，随着保温时间的增加，非热凝固区(ASZ)的厚度和结合区析出相的体积分数减小，扩散影响区(DAZ)的宽度增大。将连接温度从 1080 °C 提高到 1160 °C，保温 90 min，得到的结果相似。而且，当温度从 1080 °C 提高到 1160 °C，ASZ 的金属间化合物更快被消除。然而，继续升温至 1180 °C 后在连接区又观察到金属间化合物相。随着温度的升高，连接区宽度和母材的溶解速率增大。另外，将均匀化时间从 180 min 增加到 300 min，可消除 DAZ 中的硼化物析出相，且接头区域和母材中合金元素浓度具有较高的均匀性。

关键词：瞬时液相连接；GTD-111 高温合金；等温凝固；显微组织；均匀化

(Edited by Bing YANG)